JOURNAL OF GEOPHYSICAL RESEARCH, VOL. 103, NO. C10, PAGES 21,697–21,709, SEPTEMBER 15, 1998

Wind-wave tank measurements of bound and freely propagating short gravity-capillary waves

Martin Gade,[1] Werner Alpers,[1] Stanislav A. Ermakov,[2] Heinrich Hühnerfuss,[3] and Philipp A. Lange[4]

Abstract. Measurements of the surface elevation and slope and of the backscattered radar power at X and Ka band were carried out in a wind-wave tank with mechanically generated gravity waves as well as with wind waves on slick-free and slick-covered water surfaces. The measured radar Doppler shifts show that on a slick-free water surface, bound gravity-capillary (X and Ka band Bragg) waves are generated at the crests of steep gravity waves with frequencies between 3 and 5 Hz. However, steep gravity waves with a frequency of 2 Hz do not generate bound Ka band Bragg waves, and the Ka band backscattering from these waves is associated with wave breaking. In the wind speed range from 1.5 to 10 m/s, bound gravity-capillary waves contribute to the X and Ka band backscatter from slick-free water surfaces. The fraction of bound to freely propagating Bragg waves depends on, among other things, radar frequency, wind speed, wave amplitude of the dominant water wave, and slick coverage. In particular, the strong damping of the gravity waves by the slick at wind speeds of approximately 8 m/s leads to the disappearance of the bound Bragg waves and therefore to a reduction of the X and Ka band Doppler shifts to values corresponding to freely propagating Bragg waves. It is concluded that the study is pertinent to the understanding of former results of radar backscattering measurements in the presence of oceanic surface films.

1. Introduction

It is well known that steep gravity waves on the water surface with wavelengths less than 0.5 m can generate short gravity-capillary waves near their crests, which then propagate along the steep forward wave slopes [e.g., *Longuet-Higgins,* 1963; *Phillips,* 1977; *Plant,* 1997]. Since they do not propagate with their own phase velocity but with the (higher) phase velocity of the generating (parent) wave, they are called bound or parasitic waves. Their generation is linked to the fact that large-amplitude gravity waves have nonsinusoidal profiles and thus contain higher order harmonics. These harmonics are bound waves which, in general, do not obey the dispersion relation for free gravity-capillary waves. They propagate with the phase velocity of the 0th-order (parent) wave and since the phase velocity of these parent gravity waves is higher than the minimum phase velocity of water waves, some high-order harmonics may satisfy the dispersion relation for gravity-capillary waves. The higher order harmonics are identical to free surface waves traveling at their intrinsic phase and group velocity, and they form a wave packet moving along the steep gravity wave profile.

The generation of bound (parasitic) capillary waves (i.e., short waves which are generated at the crests of steep gravity waves and which propagate with the phase velocity of the gravity waves) has been the subject of several theoretical investigations [*Longuet-Higgins,* 1963; *Crapper,* 1970; *Ruvinsky and Freidman,* 1981; *Ruvinsky et al.,* 1991; *Longuet-Higgins,* 1992] and has also been observed in laboratory experiments [*Cox,* 1958; *Chang et al.,* 1978; *Ermakov et al.,* 1986, 1988; *Ebuchi et al.,* 1987, 1992; *Perlin et al.,* 1993; *Melville et al.,* 1995; *Rozenberg et al.,* 1996]. In this paper, we complement these measurements by addressing a problem that is of specific importance for the interpretation of radar backscatter measurements from the ocean surface, namely, when it is covered by a monomolecular slick.

According to Bragg scattering theory [*Wright,* 1968; *Valenzuela,* 1978], the backscattered radar power, which is usually measured in terms of the normalized radar cross section (NRCS or σ_0), at intermediate incidence angles is proportional to the spectral power density of water surface waves with wavelengths which are comparable to the radar wavelength. As a consequence, water wave damping by monomolecular surface films gives rise to corresponding reductions of the NRCS. Recently, radar backscattering measurements were carried out with a multifrequency/multipolarization scatterometer aboard a helicopter (called HELISCAT) over the North Sea [*Hühnerfuss et al.,* 1994, 1996; *Gade,* 1996; *Gade et al.,* 1998c; V. Wismann et al., The damping of short gravity-capillary waves by monomolecular sea slicks measured by airborne multifrequency radars, submitted to *International Journal of Remote Sensing,* 1998, hereinafter referred to as Wismann et al., 1998]. These experiments have shown that the damping of short gravity-capillary waves by oceanic surface films cannot be explained solely by Marangoni wave damping theory. Also other mechanisms contribute to the

[1]Institut für Meereskunde, Universität Hamburg, Hamburg, Germany.
[2]Institute of Applied Physics, Russian Academy of Sciences, Nizhny Novgorod, Russia.
[3]Institut für Organische Chemie, Universität Hamburg, Hamburg, Germany.
[4]Bundesanstalt für Wasserbau, Aussenstelle Küste, Hamburg, Germany.

Paper number 98JC00778.
0148-0227/98/98JC-00778$09.00

wave damping, e.g., the reduction of the wind friction velocity [*Gade,* 1996; *Gade et al.,* 1998a,c; *Wismann et al.,* 1998], the reduction of wave breaking, and the modification of nonlinear wave-wave interactions in the presence of surface films [*Alpers and Hühnerfuss*, 1989; *Gade et al.,* 1998b].

In section 2 we briefly describe the theoretical background and give a short summary of the results obtained by other investigators on the generation of parasitic capillary waves. The laboratory facility and the measuring devices are described in section 3. Experimental results on the generation of parasitic waves by mechanically generated and wind-generated gravity waves (without slicks) are presented in sections 4.1 and 4.2, respectively. The experimental results from wind-generated waves with slicks are summarized in section 4.3. The respective experimental results are discussed in sections 5.1, 5.2, and 5.3. Finally, a summary and concluding remarks are given in section 6.

2. Background

Theoretical investigations of the generation of small capillary waves at the crests of gravity waves have been carried out, for example, by *Longuet-Higgins* [1963], *Crapper* [1970], *Longuet-Higgins and Cleaver* [1994], and *Longuet-Higgins et al.* [1994]. Their results show that the surface tension at the crests of gravity waves plays an important role in the generation of bound waves by steep gravity waves. By applying a small perturbation theory, *Longuet-Higgins* [1963] has shown that the product of surface tension, τ, and local curvature at the crest of the gravity waves, κ, controls the generation of bound waves.

In laboratory experiments carried out with steep mechanically generated gravity waves (the wave steepness is defined as the ratio of wave amplitude and wavelength), it was found that the wavelength of the bound waves decreases with increasing distance from the gravity wave crest [*Chang et al.,* 1978], which is in accordance with the theory of *Longuet-Higgins* [1963]. The (intrinsic) frequencies of the bound waves were found to lie between 50 and 300 Hz. Other measurements were carried out by *Ebuchi et al.* [1987, 1992] using a 10.5 GHz (X band) scatterometer at wind speeds between 3 and 14 m/s. They also found X band Bragg waves (with wavelengths of about 3 cm) traveling with the phase velocity of the dominant waves.

The damping of small sinusoidal gravity and gravity-capillary water waves by monomolecular surface films can be explained by Marangoni damping theory [*Cini and Lombardini,* 1978; *Lucassen,* 1982; *Cini et al.,* 1983; *Alpers and Hühnerfuss,* 1989]. According to this theory, damping curves can be derived, which describe the damping of water waves by monolayers as a function of frequency. For monomolecular surface films this dependence shows a pronounced maximum at intermediate water wave frequencies (between 3 and 8 Hz) [*Cini et al.,* 1983; *Alpers and Hühnerfuss,* 1989; S.A. Ermakov et al., preprint, 1995]. Moreover, the coverage of the water surface by a surfactant leads to a reduction of the wind friction velocity and therefore to a lower energy input by the wind [e.g., *Mitsuyasu and Honda,* 1982; *Gade et al.,* 1998a]. In the presence of a monomolecular surface film the surface tension at the wave crests is also strongly reduced [*Lange and Hühnerfuss,* 1984]. As a consequence of this reduction and of the reduced steepness of the generating gravity waves, we can expect a lower generation of bound (parasitic) waves at the crests of the gravity waves. Our data show that this is indeed the case.

During our laboratory experiments, measurements of the radar backscattering were performed with two scatterometers operating at 9.8 GHz (X band) and 37 GHz (Ka band). Both scatterometers were transmitting and receiving at vertical (VV) polarization and were illuminating the water surface at intermediate incidence angles (35° and 53°, respectively). For these incidence angles the radar backscattering from the water surface can be described, to first order, by Bragg scattering theory [*Wright,* 1968; *Valenzuela,* 1978]. According to this theory, the normalized radar cross section (NRCS) is proportional to the spectral power density of the Bragg waves, that is, of those surface waves of wavelengths λ_B that obey the Bragg resonance condition

$$\lambda_B = \frac{\lambda_0}{2 \sin \vartheta} \quad , \tag{1}$$

where λ_0 denotes the radar wavelength and ϑ denotes the incidence angle. For a slick-free water surface the NRCS σ_0 can be written as

$$\sigma_0 = |g_{VV}|^2 16\pi k_0^4 \cos^4 \vartheta \cdot \Psi(k_B) \quad , \tag{2}$$

where k_0 denotes the radar wavenumber and $\Psi(k_B) = \frac{1}{2}[E(\vec{k}_B)+E(-\vec{k}_B)]$ denotes the spectral power density of the Bragg waves, with wavenumber $k_B = 2\pi/\lambda_B$, which are propagating in and against the antenna look direction. The function $|g_{VV}|^2$ is the so-called Bragg coefficient for vertical transmission and reception, and it depends on radar wavenumber, the relative dielectric constant, ε, between the water and the air, and incidence angle [see *Valenzuela,* 1978].

3. Experimental Setup

All of the measurements reported herein were carried out in the wind-wave tank facility of the University of Hamburg. The tank is 26 m long and 1 m wide. It is filled with freshwater and has a mean water depth of 0.5 m. The wind tunnel height is 1 m, and the effective (maximum) fetch is 19 m. All of the measurements reported herein were performed at a fetch of 15.5 m. Wind speeds up to 25 m/s are generated by a radial blower, while mechanical waves with frequencies between 0.7 and 2.5 Hz are generated by a wave flap. In the experiments reported herein, mechanical waves with frequencies above 2.5 Hz were generated using a wave follower that was converted to a wave generator by attaching a Styrofoam paddle to it and by driving it with a sinusoidal power input. The wave generator was mounted on the roof of the tank 4 m upwind of the measuring area.

The wind-wave tank has a beach for wave damping at the leeward end (see Figure 1). In the measurement area (where the footprints of both radars and the wave gauges are located), the metallic plates of the tank's roof were replaced by Styrofoam diagrams to ensure the unattenuated transmission of the microwaves. Plates of microwave-absorbing material were attached to the Styrofoam diagrams in the direction of the specular-reflected radar beams (see Figure 1). For more detailed information about the wind-wave tank the reader is referred to the work of *Hühnerfuss et al.* [1976].

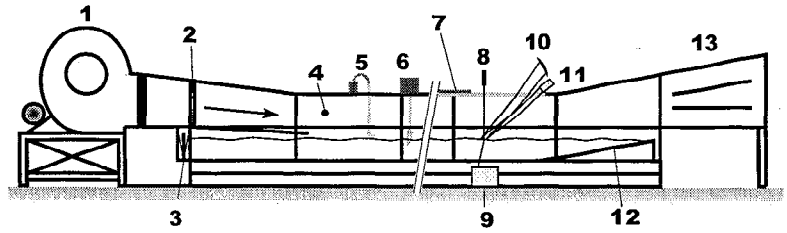

Figure 1. Schematic side view of the wind-wave tank of the University of Hamburg. The numbers denote the Following 1, blower; 2, honeycomb for producing laminar airflow; 3, wave flap; 4, anemometer; 5, pump and pipette; 6, wave follower; 7, Styrofoam and absorber; 8, laser and wire; 9, laser optic; 10, X band antennae; 11, Ka band; 12, beach and overflow baffle; and 13, diffuser.

In order to simulate reliably the morphological structure of natural sea slicks [*Hühnerfuss et al.*, 1996], monomolecular slicks were produced by distributing oleyl alcohol (OLA) on the water surface by using the spreading solvent ethanol. A 75 mmol/L solution was deployed at 5.5 m fetch, applying a pipette that was fixed such that the drops fell from a height of a few millimeters without plunging deeply below the water surface. This allowed for the optimum spreading of the monolayer without significant losses to the bulk water. The films were transported by waves and/or wind toward the leeward end of the tank. A minimal overflow was maintained with a permanent water inflow at the windward end of the tank (Figure 1).

The radar measurements were performed with two upwind looking radar antennae for transmission and reception. We used a coherent continuous wave (CW) 9.8 GHz (X band) scatterometer of the University of Hamburg, operating at an incidence angle of 35°. The X band microwave beam was focused on the water surface by means of a bistatic parabolic reflector construction mounted on a metal frame that was fixed to the roof of the hall where the wind-wave tank is located. Additionally, a CW 37 GHz (Ka band) scatterometer of the Russian Academy of Sciences, operating at an incidence angle of 53°, was used in this experiment. The Ka band microwave beam was focused on the water surface by using a plastic lens. The dimensions of the X and Ka band radar footprints at the water surface were 16 cm × 12 cm and 32 cm × 19 cm, respectively. The parameters of both scatterometers are listed in Table 1.

Wave heights were measured using a resistant-type wire wave gauge [*Lobemeier*, 1981] with a 0.075 mm diameter tungsten wire whose penetration point into the water was located at a distance of 22 cm laterally from the footprints of the scatterometer antennae (i.e., at the same fetch length). Wave slopes were measured using a laser slope gauge [*Lange et al.*, 1982] whose footprint was in the center of the footprints of the scatterometer antennae. The frequency resolutions of the wire gauge is 30 Hz, and that of the laser slope gauge is better than 100 Hz. The reference wind speed U_{ref} was measured at the wind entrance 65 cm above the mean water surface level using a propeller-type anemometer.

4. Results

The influence of the coverage of the water surface by monomolecular surface films on the measured wave spectra as well as on the radar backscatter was already investigated in wind-wave tank experiments by *Hühnerfuss* [1986], *Hühnerfuss et al.* [1981, 1982, 1987], *Feindt* [1985], *Gade* [1996], and *Gade et al.* [1998a] using mechanically-generated as well as wind-generated waves. With the present investigation we complement earlier measurements by addressing a new problem that seems to be of relevance to wave damping by biogenic slicks floating on the ocean surface. The measurements reported herein were carried out in three steps: (1) generation of bound (parasitic) waves by mechanically generated gravity waves on a slick-free water surface, (2) generation of bound waves by wind-generated waves on a slick-free water surface, and (3) generation of bound waves by wind-generated waves on a water surface covered with OLA.

4.1. Mechanically Generated Waves

In a first step we studied the generation of bound (parasitic) waves at the crests of gravity waves that were mechanically generated. For this purpose we used the above mentioned converted wave follower for waves with frequen-

Table 1. Parameters of the Two Scatterometers Used in the Experiment and the Parameters of the Bragg Waves

	Radar Band	
	X	Ka
Frequency, GHz	9.8	37.0
Wavelength, cm	3.06	0.81
Polarization	VV	VV
Beam focusing, cm	bistatic parabolic reflector (Ø 56)	plastic lens (Ø 10)
Antenna pattern (range/azimuth), deg	4 / 3 (1-way, 3 dB)	6 (2-way, 3 dB)
Incidence angle, deg	35	53
Footprint size (range/azimuth), cm × cm	16 × 12	32 × 19
Bragg wavelength, cm	2.67	0.51
Bragg wavenumber, rad/m	235	1239
Phase velocity of Bragg waves, cm/s	24.3	31.4

Table 2. Parameters of the Mechanically Generated Waves

	Wave Frequency, Hz			
	2	3	4	5
Wavelength, cm	39.1	17.5	10.0	6.7
Wave generator	wave flap	converted wave follower	converted wave follower	converted wave follower
Mean amplitude range, cm	0.16 – 1.30	0.06 –0.66	0.02 – 0.33	0.02 – 0.15
Threshold amplitude, cm	~ 0.60	~ 0.32	~ 0.18	~ 0.11
Threshold steepness	~ 0.015	~ 0.018	~ 0.018	~ 0.017

cies of 5, 4, and 3 Hz, and we used the wave flap for waves with a frequency of 2 Hz. For each wave frequency the amplitude range was chosen in such a way that the threshold amplitude (i.e., the amplitude where the generation of bound waves was measured) was well covered. In Table 2 the wavelengths and amplitude ranges as well as the experimental values for the threshold amplitude and threshold steepness (i.e., the ratio of the threshold amplitude and the wavelength) are listed.

Figure 2 shows the slope spectra of those waves that were generated by the converted wave follower oscillating at a fixed frequency of 4 Hz but having variable amplitudes. The mean amplitudes of the 4 Hz (basic) waves are inserted into each diagram. Figures 2a and 2b are obtained at amplitudes lower than the threshold value (for the generation of bound waves), and Figures 2c and 2d are obtained at amplitudes higher than the threshold value (see Table 2). For low amplitudes the spectra contain quasi-discrete harmonics of the (steep) gravity waves, whereas at the threshold amplitude the discrete spectrum changes to a continuous spectrum. For amplitudes higher than the threshold value a region of reduced falloff in the slope spectrum can be delineated in Figures 2c and 2d between 60 and 100 Hz. This region is followed by a cutoff in the spectrum at frequencies above 100 Hz. It is worth noting that the threshold steepness has almost the same value for all wave frequencies (see Table 2).

The results reported herein show that there exists a threshold amplitude of the 4 Hz gravity waves, where the generation of bound waves starts (approximately 0.2 cm in our measurements; see Table 2). This behavior confirms the previous results of *Ermakov et al.* [1986], who observed a threshold-like excitation of parasitic capillary ripples by gravity waves (when these gravity waves are steep enough). Following *Donelan and Hui* [1990 and references therein], the transition from a discrete to a continuous spectrum results from an instability of the gravity waves [*Mc Lean,* 1982]. Manifestations of this modulational instability [*Benjamin and Feir,* 1967] are the sideband peaks adjacent to the fundamental frequency (see Figures 2c and 2d). *Ermakov et al.* [1986] concluded from their measurements that the dominant parasitic waves have frequencies between 60 and 80 Hz. The spectra measured at amplitudes higher than the threshold value (see Table 2)show significantly enhanced energy in the 60–80 Hz band (see Figure 2), which can be attributed to bound (parasitic) waves. It is worth noting that this region of reduced falloff is most prominent for wave frequencies between 5 and 4 Hz. For 2 Hz waves (not shown here) this peculiarity is absent, which we interpret as a consequence of the fact that 2 Hz waves do not

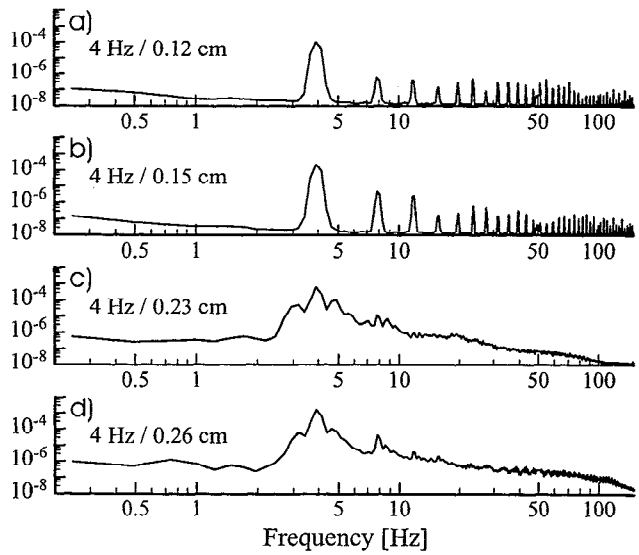

Figure 2. Slope spectra of water waves mechanically generated by the converted wave follower with a frequency of 4 Hz and varying amplitudes. For (a) and (b) the wave amplitudes (0.12 and 0.15 cm) are smaller than the threshold amplitude for the generation of bound waves. For (c) and (d) the amplitudes (0.23 and 0.26 cm) are larger than the threshold amplitude (see Table 2).

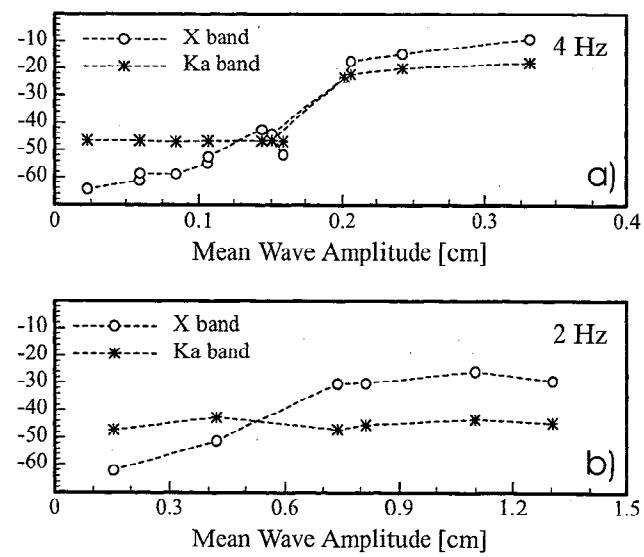

Figure 3. Relative backscattered power (RBP) from the water surface measured at X and Ka band, vertical (VV) polarization measured in the wind-wave tank with the antennae looking against the propagation direction of the waves. The RBP is plotted as a function of the amplitude of the (parent) gravity wave with a frequency of (a) 4 Hz and (b) 2 Hz.

generate parasitic capillary ripples, at least under the present experimental conditions.

As examples for the relative backscattered power (RBP) at X and Ka band the results measured at wave frequencies of 4 and 2 Hz and at wave amplitudes between 0.25 and 3.2 cm are shown in Figure 3. We found that for frequencies of 3, 4, and 5 Hz, the dependence of the backscattered radar power at X and Ka band on the mean wave amplitude strongly increases near the threshold amplitude (about 0.18 cm in the case of 4 Hz waves; see Figure 3a) and saturates or increases very slowly for larger amplitudes. For the 2 Hz wave (Figure 3b) the increase in the X band RBP with mean wave amplitude is less pronounced, and for the Ka band there is no increase. The X and Ka band Doppler spectra shown in Figure 4 and Figure 5, respectively, were measured at amplitudes higher than the threshold values (compare Table 2). The (mean) propagation velocity of the respective scatterers is shown on the horizontal axis at the top of Figures 4 and 5. Moreover, the solid vertical lines included into each diagram denote the theoretical Doppler shift for freely propagating Bragg waves. For 3, 4, and 5 Hz waves the maxima in the X and Ka band Doppler spectra do not correspond to the phase velocities of freely propagating Bragg waves (24.3 and 31.4 cm/s, respectively) but to a higher propagation velocity (see section 5.1). A broad spectral signal at negative frequencies in the X band Doppler spectrum was found for the 3 Hz gravity waves. A comparable Doppler signal was also measured by *Keller et al.* [1974], who interpreted it as being caused by Bragg waves, which propagate in the opposite direction as the mechanically generated waves and which result from reflections of the gravity waves at the tank beach. However, the X band Doppler spectrum for the 2 Hz waves exhibits a new feature. In addition to the high-frequency peak described above, a low-frequency peak appears at a Doppler frequency of about 5 Hz (see Figure 4d). In the Ka band Doppler spectrum, no such peak can be delineated at the corresponding Doppler frequency (about 80-100 Hz, see Figure 5). This finding is in accordance with our assumption that bound capillary waves are effectively not generated by gravity waves, which have (intrinsic) frequencies lower than approximately 2.5 Hz, that is, wavelengths longer than 25-30 cm. Instead of a spectral peak at about 80–100 Hz, a peak appears at a (low) frequency of about 30 Hz. These low-frequency peaks in both the Ka band and the X band Doppler spectra result from scatterers having the same propagation velocity (about 15 cm/s).

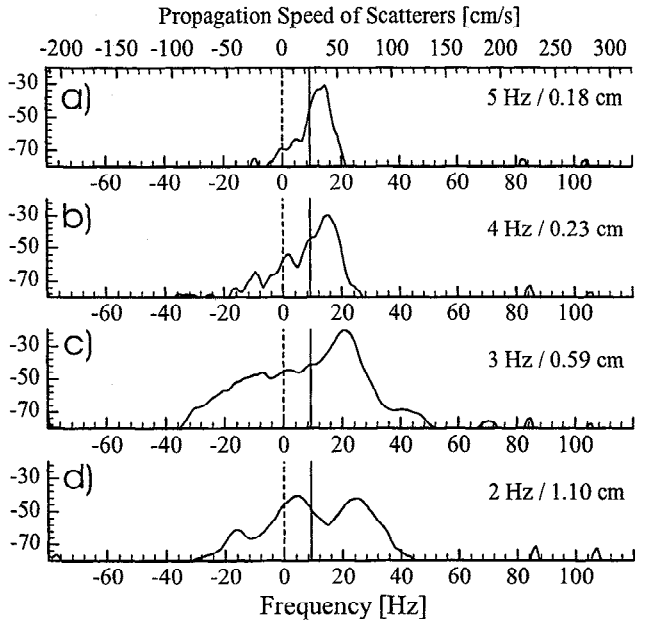

Figure 4. X band Doppler spectra for mechanically generated waves of different frequencies and amplitudes. In all cases the wave amplitude is higher than the threshold value for the excitation of bound waves. The scale at the top shows the corresponding propagation velocity of the scatterers (see equation (3)). The solid vertical lines included into each diagram denote the theoretical Doppler shift for freely propagating Bragg waves.

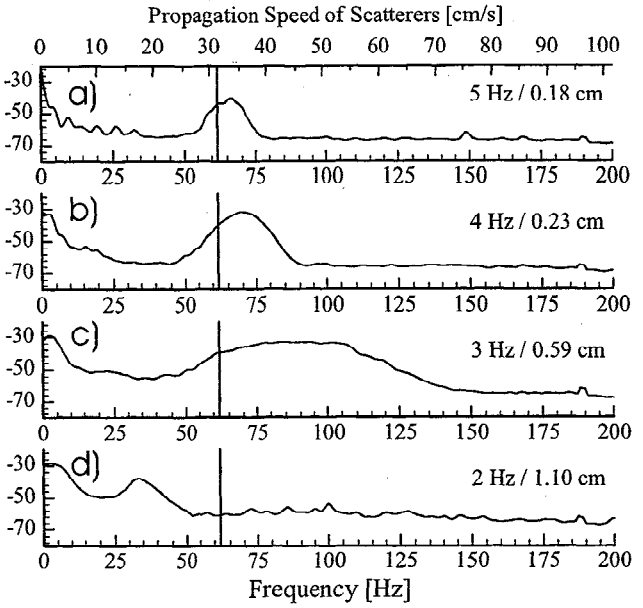

Figure 5. Same as Figure 4 but for Ka band Doppler spectra.

4.2. Wind Waves Without Slicks

As a next step, we expand the results obtained with mechanically generated gravity waves to the (more realistic) case of wind-generated waves. In order to investigate whether or not the results presented in section 4.1 can be transferred to wind-generated waves, we performed the measurements at wind speeds between 1.5 and 10 m/s. Figure 6 shows the dependence of the frequency, mean amplitude, and downwind slope of the dominant wave on wind speed (Figures 6a, 6b, and 6c, respectively). The frequency of the dominant wave was obtained by calculating the first moment of the wave height spectrum measured with the wire gauge. The amplitudes and slopes of the dominant waves were obtained by integrating the corresponding spectral peaks of the amplitude and slope spectra, within their 3 dB limits, respectively. At a wind speed of 2 m/s the frequency of the dominant wave is larger than 5 Hz and decreases to 2 Hz at a wind speed of approximately 9 m/s. Thus the frequency range of the mechanically generated gravity waves used in the experiments described in section 3 is the same as the range of the frequencies of the dominant waves at wind speeds between 2 and 10 m/s. Note the strong increase in the downwind slope (Figure 6c) at wind speeds between 1.5 and 3 m/s and the saturation or weak

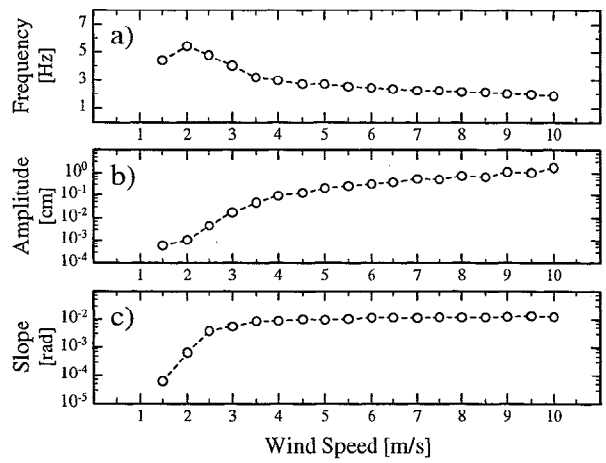

Figure 6. Dependence of the (a) frequency, (b) mean amplitude, and (c) mean downwind slope of the dominant wave in the wind wave spectrum on wind speed.

increase in the downwind slope above 3 m/s. This behavior corresponds to an increase in the high-frequency part of the downwind slope spectra shown in Figure 7. At wind speeds of 4, 6, and 8 m/s the slope spectra exhibit a reduced falloff at frequencies above 10 Hz, and they exhibit a stronger falloff at frequencies above approximately 80 Hz. This is in agreement with the wave spectra of *Jähne and Riemer* [1990] and *Apel* [1994]. Note that these features are similar to those obtained for the 3-5 Hz mechanically generated waves at amplitudes higher than the threshold value (compare Figure 2; however, caution has to be applied when comparing the slope spectra for mechanically generated and wind-generated waves, since the laser slope gauge measures "spectra of encounter"). We will show in section 5.2 that this can be interpreted as a manifestation of the generation of bound waves.

The X and Ka band Doppler spectra measured at different wind speeds are depicted in Figures 8 and 9, respectively. Again, the solid vertical lines included in each diagram denote the theoretical Doppler shift for freely propagating Bragg waves (the increase in this Doppler shift with wind speed is due to the wind-induced surface drift; see below). At a wind

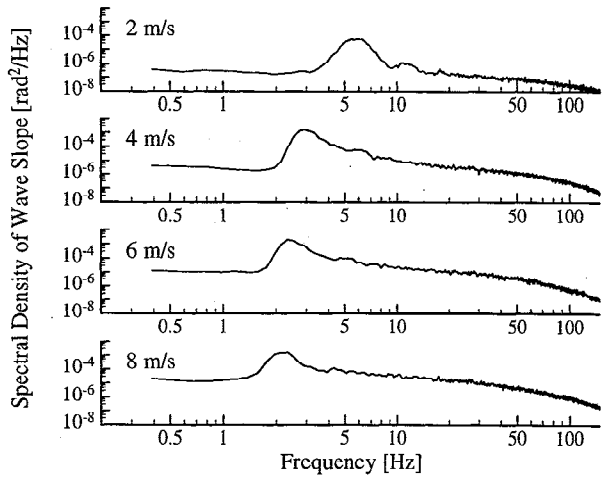

Figure 7. Slope spectra of wind-generated waves at different wind speeds measured in the wind-wave tank on a slick-free water surface.

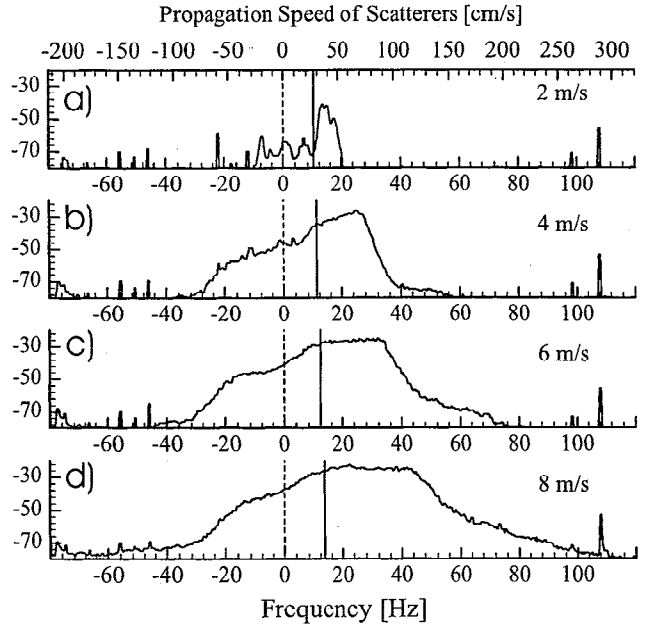

Figure 8. X band Doppler spectra at different wind speeds measured in the wind-wave tank when the water surface is slick-free. The scale at the top shows the corresponding propagation velocity of the scatterers (see equation (3)). The solid vertical lines included into each diagram denote the theoretical Doppler shift for freely propagating Bragg waves (taking into account the wind-induced surface drift).

speed of 2 m/s, corresponding to a wind friction velocity, u_*, of 11.7 cm/s (Figures 8a and 9a) the locations of the maxima in the Doppler spectra (Doppler peaks) agree well with those measured for mechanically generated waves with a frequency of 5 Hz (13 and 67 Hz at X and Ka band, respectively; see Figures 4a and 5a). At a wind speed of 4 m/s ($u_* = 24.2$ cm/s) the Doppler peaks lie in the same frequency range as those obtained from 3 Hz mechanically generated waves (Figures 4

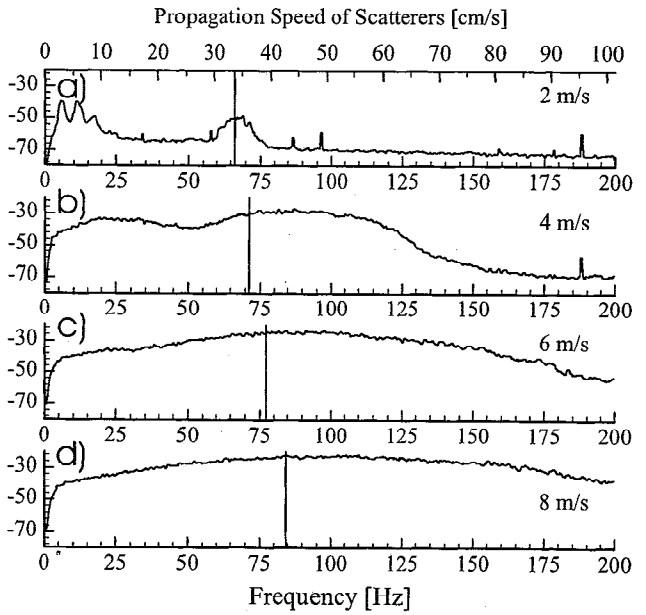

Figure 9. Same as Figure 8 but for Ka band.

and 5); however, they are broader for the wind-generated waves. At wind speeds above 4 m/s ($u_* > 24.2$ cm/s) the spectral peak in the X band Doppler spectra is broadened, a finding that can be explained by the superposition with an additional spectral peak at about 10 Hz (propagation velocity of 26.7 cm/s), corresponding to free wind-generated X band Bragg waves. The Ka band Doppler spectra for $U_{ref} > 4$ m/s are broad and do not clearly exhibit the presence of a (second) low-frequency peak at about 65 Hz, corresponding to the peak in the X band Doppler spectrum.

4.3. Wind Waves With Slicks

The third step of our measurements was to investigate the influence of a slick coverage of the water surface on the generation of the different kinds of Bragg waves (bound or freely propagating). For this purpose, another set of measurements was performed in the wind-wave tank with a water surface covered with OLA. The influence of the coverage of the water surface by monomolecular surface films has already been investigated by *Gade et al.* [1998a], who found that on a slick-covered water surface no (wind generated) waves were measured at wind speeds lower than 4 m/s. Thus we concentrated on the wind speed range between 4 and 10 m/s for our measurements with slick-covered water surfaces.

The Doppler spectra recorded at X and Ka band are depicted in Figures 10 and 11, respectively, for wind speeds of 4, 6, 8, and 10 m/s (corresponding to wind friction velocities between 15.2 and 38.0 cm/s). The solid vertical lines included into each diagram denote the theoretical Doppler shift for freely propagating Bragg waves. (Owing to a reduced wind friction velocity and thus to a reduced surface drift, the theoretical Doppler shifts are smaller than those calculated for the same wind speed and a slick-free water surface.) At 4 m/s the peak in the X band Doppler spectrum measured from a slick-covered water surface is very narrow. However, the Doppler spectrum shows features qualitatively similar to those of the spectrum obtained from a slick-free water surface at 2 m/s (see Figure 8; in comparing the Doppler spectra a lower wind speed has to be taken in the case of a slick-free water surface because u_* is reduced when the water surface is covered with a slick [e.g., *Mitsuyasu and Honda,* 1982]). At the wind speeds of 6 and 10 m/s, the X and Ka band Doppler spectra from a slick-covered water surface are in qualitative agreement with those for a slick-free water surface at 4 and 8 m/s (see Figures 8 and 9, respectively). We interpret this as being due to the reduction of the wind friction velocity in the presence of the monomolecular slick [*Mitsuyasu and Honda,* 1982; *Wei and Wu,* 1992; *Gade et al.,* 1998a], which causes a reduced generation of wind waves [see *Plant,* 1982]. The most prominent differences between the Doppler spectra at a slick-covered and a slick-free water surface, both at X and Ka band, are found to be at intermediate wind speeds, that is, at 8 m/s (slick covered) and 6 m/s (slick free); at a slick-covered water surface we measured narrow Doppler peaks (with corresponding reductions of the mean Doppler shifts), whereas at a slick-free water surface the Doppler spectra become broader with increasing wind speed.

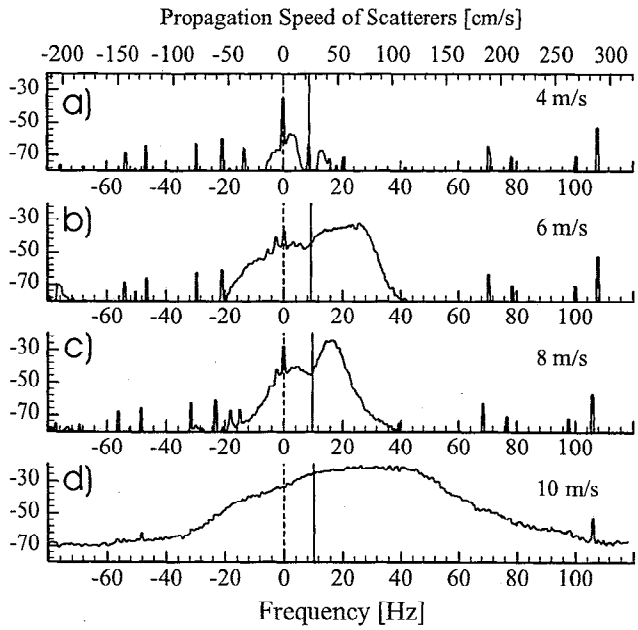

Figure 10. X band Doppler spectra at different wind speeds measured in the wind-wave tank on a water surface covered with oleyl alcohol (OLA). The scale at the top shows the corresponding propagation velocity of the scatterers (see equation (3)). The solid vertical lines included into each diagram denote the theoretical Doppler shift for freely propagating Bragg waves (taking into account the wind-induced surface drift).

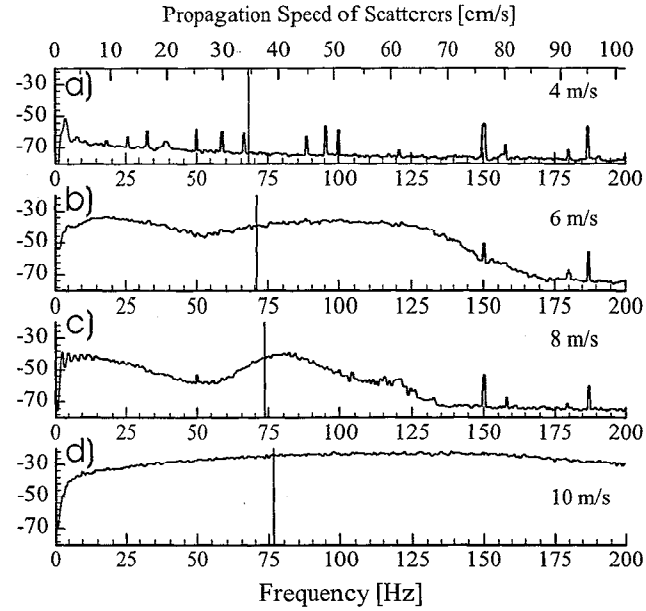

Figure 11. Same as Figure 10 but for Ka band.

5. Discussion

5.1. Mechanically Generated Waves

The results obtained in the experiments with mechanically generated 2 Hz waves are qualitatively and quantitatively different from those obtained from 3–5 Hz waves. In particular, the region of reduced falloff at wave frequencies between 60 and 100 Hz (see Figure 2) is absent, which we interpret as a consequence of the fact that 2 Hz waves do not generate parasitic capillary ripples.

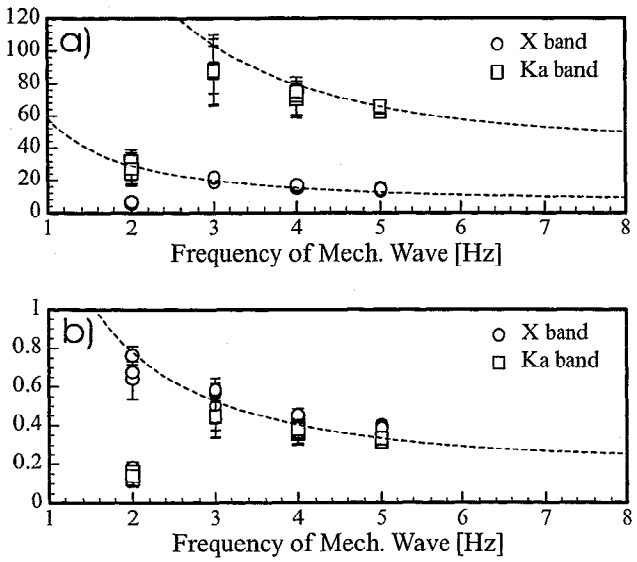

Figure 12. (a) Measured Doppler shifts at X and Ka band and (b) mean velocity of the scatterers derived from these Doppler shifts. The dashed curves are obtained by assuming that only bound waves cause the radar backscattering.

However, as described in section 3, the 2 Hz waves were generated by using the wave flap, whereas the 3, 4, and 5 Hz waves were generated by using the (vertical moving) converted wave follower. This could imply that the generation of bound waves depends on the wave generation mechanism. However, from an additional measurement carried out with 3 Hz waves generated by the wave flap, we obtained practically the same results as we obtained with the wave follower. We are, therefore, quite confident that the wave generation mechanism itself is not responsible for the observed differences between the waves of different frequencies. Moreover, the higher order wave form, like skewness and kurtosis, may also affect the curvature of the gravity waves, which is important for the generation of parasitic capillary waves [*Longuet-Higgins,* 1963].

Figure 12 shows the mean Doppler shifts, f_d, and the mean propagation velocities, c_m, calculated from the X and Ka band Doppler spectra of mechanically generated waves (Figures 4 and 5, respectively), as functions of the frequency of the mechanically generated gravity waves, f_g. The dashed curves in Figures 12a and 12b denote the theoretical values, which were obtained by assuming that the Bragg waves propagate with the phase velocity of the gravity waves, $c(f_g)$; that is, the relationship between this phase velocity and the measured Doppler shift, f_d, is

$$2\pi f_d = 2k_0 \sin\vartheta \cdot c(f_g) \tag{3}$$

where f_g denotes the gravity wave frequency. The theoretical Doppler shifts derived by using (3) are in good agreement with the measured ones (Figure 12a). For a better comparison, the mean propagation velocities of the X and Ka band Bragg waves, derived from the measured Doppler shifts by using (3), are plotted in Figure 12b. It is obvious that for the mechanically generated waves with frequencies between 3 and 5 Hz, the radar backscattering at X and Ka band is caused by scatterers which propagate with the phase velocity of the gravity waves; that is, they are not freely propagating waves but bound harmonics or parasitic waves. The X band backscatter from 2 Hz waves is obviously caused by two different scatterers. As described in section 4.1, the high-frequency peak (see Figure 4d) corresponds to Bragg waves bound to the 2 Hz gravity wave. Both the low-frequency peak in the X band Doppler spectrum and the peak in the Ka band Doppler spectrum (Figure 5d) correspond to a propagation velocity of the scatterers of about 15 cm/s. As *Kwoh and Lake* [1985] have shown in a similar experiment, this peak can be interpreted as being caused by the turbulent wake generated by the breaking gravity waves and convected by the orbital velocity of the gravity waves. If the relaxation time of the turbulent patches formed by the breaking crests is smaller than the period of the gravity wave, one can expect that a peak will occur in the radar Doppler spectrum at a frequency corresponding to the orbital velocity. In our case (i.e., for 2 Hz waves with amplitudes higher than the threshold value (between 0.6 and 1.3 cm)), the orbital velocity of the gravity wave is in the range between 12 and 15 cm/s. We therefore conclude that the situation described above was encountered in our experiments.

5.2. Wind-Generated Waves Without Slicks

The wind speed dependence of the downwind slope (Figure 6c) at low to moderate wind speeds (up to approximately 5 m/s) can be explained by assuming that the wave slopes in the downwind direction are determined by the slope of the short gravity waves and the bound (parasitic) capillary waves propagating with the phase velocity of the short gravity waves. At a wind speed of 4-5 m/s the frequency of the dominant wave is lower than 3 Hz, and waves of this frequency cannot effectively generate bound waves. Thus the mean wave slope does not increase significantly beyond this wind speed.

The locations of the maxima in the X and Ka band Doppler spectra at the wind speed of 2 m/s (Figures 8a and 9a) agree well with those measured for mechanically generated waves with a frequency of 5 Hz (Figures 4a and 5a). The dominant frequency at a wind speed of 2 m/s is approximately 5 Hz. Thus we conclude that the Bragg waves at this wind speed are bound to the dominant wind waves. A similar wind speed dependence of the X band Doppler spectra was observed in laboratory experiments by *Kwoh and Lake* [1985].

Figure 13 shows the mean X and Ka band Doppler shifts calculated from the corresponding Doppler spectra (Figures 8 and 9, respectively). Following *Ebuchi et al.* [1992], the propagation velocity, c, of the scatterers which are bound to the dominant gravity waves can be written as

$$c = \frac{g}{\omega_{\mathrm{dom}}} + 0.2 \cdot u_*, \tag{4}$$

where g denotes the acceleration of gravity, $\omega_{\mathrm{dom}} = 2\pi f_{\mathrm{dom}}$ denotes the radian frequency of the dominant wave, and u_* denotes the wind friction velocity. The second summand on the right-hand side of (4) describes the "effective drift velocity" given by *Tokuda and Toba* [1982]. The theoretical curves inserted into Figures 13a and 13b are calculated assuming that only bound waves (dashed curves) or only freely propagating Bragg waves (solid curves) are responsible for the radar backscattering (see equation (4)). The dashed curves correspond to bound Bragg waves (taking into account (3) and (4)),

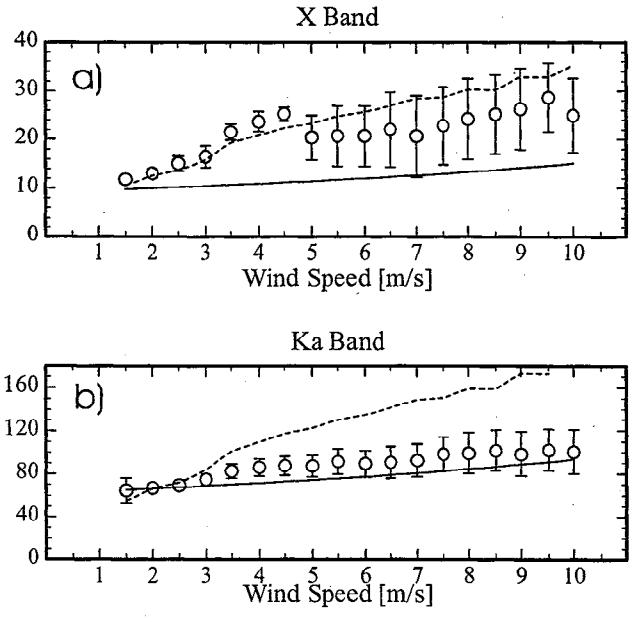

Figure 13. Wind speed dependence of the mean Doppler shifts at (a) X band and (b) Ka band. The two theoretical curves inserted into Figures 1^3a and 13b are calculated by assuming that only bound waves (dashed curves) or only freely propagating Bragg waves (solid curves) are responsible for the radar backscattering (see equation (4)).

whereas the solid curves correspond to Bragg waves propagating with the sum of their own phase velocity and the effective drift velocity (the wind friction velocities were taken from *Gade et al.* [1998a]). The measured X band Doppler shifts at wind speeds below 5 m/s ($u_* < 31.3$ cm/s) agree quite well with the theoretical ones for bound Bragg waves (see the dashed curve in Figure 13a). At 5 m/s ($u_* = 31.3$ cm/s) the measured X band Doppler shifts drop to lower values, and at higher wind speeds they are significantly lower than the theoretical values for bound Bragg waves but are still higher than those calculated for freely propagating waves. These results agree well with those obtained for mechanically generated waves; at low to moderate wind speeds (up to approximately 5 m/s), where the frequency of the dominant wind waves is higher than 2.5 Hz (see Figure 6), the X band Bragg waves are mostly bound to the dominant waves, whereas at higher wind speeds the Bragg waves are a mixture of bound and freely propagating waves [see also *Plant*, 1997]. This explains the observed drop of the measured Doppler shifts at about 5 m/s.

In the entire wind speed range considered in our experiments, the measured Ka band Doppler shifts increase slowly with wind speed (Figure 13b), and they are significantly smaller than the calculated values for bound waves at wind speeds above 3 m/s ($u_* > 17.8$ cm/s). At low wind speeds (2–3 m/s) the Ka band Bragg waves cannot easily be separated into bound and freely propagating waves because their phase velocity is comparable to that of the dominant wind wave (see Figure 13). However, with respect to the results obtained for mechanically generated waves, our experimental data suggest that at low to moderate wind speeds (up to about 4.5 m/s) the Ka band Bragg waves are a mixture of bound and freely propagating waves, whereas at higher wind speeds they are presumably freely propagating waves.

Note that these results are not in agreement with the results obtained by *Keller et al.* [1974] and by *Graf et al.* [1977] in wave tank measurements in which they employed coherent X and Ka band scatterometers. In particular, *Graf et al.* [1977] concluded that the radar backscattering at intermediate incidence angles is determined by freely propagating wind waves rather than by parasitic waves. Very likely, the discrepancy between their and our results can be attributed to the fact that these authors used shorter fetches, and thus the amplitudes of their wind-generated gravity waves were smaller than the threshold values for the generation of bound waves. This is in accordance with the results obtained by *Melville et al.* [1995], who found that the radar backscattering by bound capillary waves increases as wind and fetch increase. On the other hand, *Duncan et al.* [1974] and *Ebuchi et al.* [1987, 1992] claimed that in the entire wind speed range between 3.8 and 13.7 m/s, X band Bragg waves are bound waves. In contrast to our experiments, they used an incoherent X band scatterometer and obtained their results from the analysis of the time series of the backscattered radar power. The discrepancy between their and our results may therefore be due to the different experimental setups and the different data analyses. The use of a coherent radar system, however, seems to yield more reliable results, particularly, measurements of the propagation velocity of the scatterers. On the other hand, our results are in qualitative agreement with those of *Ebuchi et al.* [1993], who found in their time series analyses of the backscattered radar power that only the Bragg waves at the crests of the gravity waves propagate with the phase velocity of these gravity waves, whereas the Bragg waves at the wave troughs propagate with a lower velocity. This result also implies the existence of two different kinds of Bragg waves.

The radar backscattering from turbulent wakes, as was observed in our experiments with the mechanically generated 2 Hz waves (see section 5.1), seems to be unimportant for wind speeds below 7 m/s ($u_* < 47.7$ cm/s), when the dominant waves do not break. At a wind speed of approximately 7 m/s the waves in the wind-wave tank start breaking [*Feindt*, 1985]. Although a pronounced Doppler peak at low frequencies cannot be inferred from the measured Doppler spectra at 8 m/s (Figures 8d and 9d), we hypothesize that radar backscattering from turbulent wakes also contributes to the measured Doppler spectra at wind speeds above 7 m/s.

5.3. Wind-Generated Waves With Slicks

Figure 14 shows the wind speed dependence of the mean X and Ka band Doppler shifts for a water surface covered with OLA. The mean Doppler shifts have been derived from the X and Ka band Doppler spectra depicted in Figures 10 and 11, respectively. Again, the theoretical curves inserted into Figures 14a and 14b are calculated assuming that only bound waves (dashed curves) or only freely propagating Bragg waves (solid lines) are responsible for the radar backscattering (see equation (4)). Since the wind friction velocity is reduced in the presence of a monomolecular surface film, the effective drift velocity given by *Ebuchi et al.* [1992] is also reduced (see equation (4)). As a consequence, the slope of the theoretical curves in Figures 14a and 14b is smaller than that for slick-free water surfaces (see Figures 13a and 13b). It can be deduced from the measured X band Doppler shifts (Figure 14a) that at 5 m/s the X band Bragg waves are predominantly freely propagating (however, only very few Bragg waves are

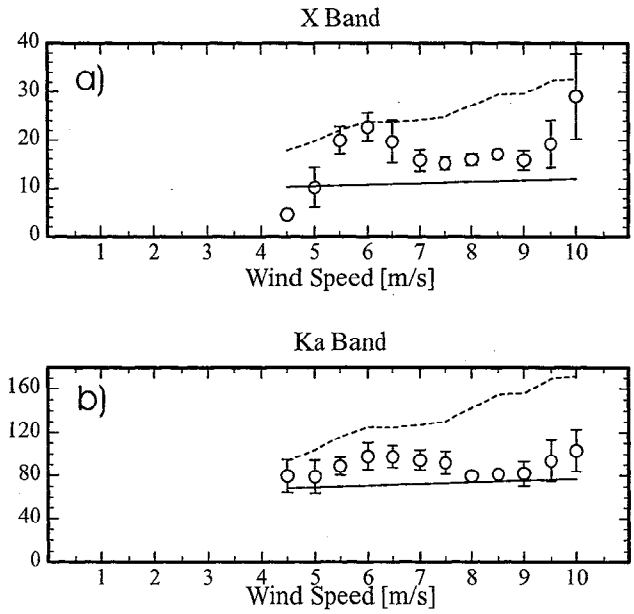

Figure 14. Wind speed dependence of the mean Doppler shifts at (a) X band and (b) Ka band, measured on a water surface covered with oleyl alcohol (OLA). The two theoretical curves inserted into Figures 14a and 14b are calculated by assuming that only bound waves (dashed curves) or only freely propagating Bragg waves (solid curves) are responsible for the radar backscattering (see equation (4)).

generated at that wind speed). At approximately 6 m/s, also longer (gravity) waves are generated by the wind, which in turn generate bound waves at their crests. The radar backscattering by the mixture of both kinds of Bragg waves leads to a broadening of the Doppler spectrum (see Figure 10). However, from the position of the peak maximum it can be inferred that at 5 m/s the radar backscattering at X band is mainly caused by bound Bragg waves. At 7–9 m/s we measured a strong reduction of the X band Doppler shifts to values corresponding to freely propagating Bragg waves. In this wind speed range the short gravity waves are strongly damped by the slick, so that no bound waves can be generated (we also measured a strong reduction of the root-mean-square surface elevation and surface slope, which is not shown herein). At approximately 9.5 m/s the slick starts to disperse, so that the measured Doppler shifts correspond to those measured on a slick-free water surface (compare Figure 13).

From the measured Ka band Doppler shifts (Figure 14b) the same qualitative results can be inferred as from the X band Doppler shifts. Again, a mixture of bound and freely propagating Bragg waves is responsible for the Ka band backscattering at intermediate wind speeds (approximately 6 m/s; see Figure 11). At 8 m/s, lower Ka band Doppler shifts (corresponding to freely propagating Bragg waves) are measured; thus at this wind speed only freely propagating Ka band Bragg waves are present.

The disappearance of bound Bragg waves in the wind speed range between 7 and 8 m/s causes narrow peaks in the measured X and Ka band Doppler spectra (see the spectra obtained at 8 m/s, shown in Figures 10c and 11c). In turn, these narrow Doppler peaks result in smaller error bars of the measured Doppler shifts shown in Figure 14. As in the case of slick-free water surfaces (see Figure 8), the radar backscatter from a mixture of two kinds of scatterers moving with (slightly) different velocities leads to a broadening of the maxima in the measured Doppler spectra. If one of these two kinds of scatterers (e.g., the bound Bragg waves) is absent, only a narrow Doppler peak at a frequency corresponding to the propagation velocity of the remaining scatterers (i.e., of freely propagating Bragg waves) is measured. Moreover, the absence of bound Bragg waves in the wind speed range between 7 and 8 m/s results in a strong reduction of the radar backscattering (as already measured by *Feindt* [1985] and *Gade et al.* [1998a]). The wind speed dependence of the measured damping ratios, that is, the ratios of the backscattered radar power from a slick-free and a slick-covered water surface, both at X and Ka band, is plotted in Figure 15. In addition, the theoretical damping ratios are shown as dashed horizontal lines. These values were calculated assuming pure Marangoni damping [*Hühnerfuss,* 1986] of (freely propagating) Bragg waves. (Marangoni damping theory predicts for OLA a maximum wave damping at 4.9 Hz and a decrease in the damping ratio at higher wave frequencies. Thus the theoretical damping ratio is smaller for Ka band Bragg waves than for X band Bragg waves.) In Figure 15 there is a slight maximum of the X band damping ratios in the wind speed range between 6 and 8 m/s, which coincides with the strong decrease in the measured X band Doppler shifts at that wind speed (see Figure 14a). Again, this damping maximum can be related to the strong damping of bound X band Bragg waves (with respect to the slick-free water surface), which is in accordance with the above interpretation of the measured X band Doppler shifts.

The maximum of the Ka band damping ratios is also found in the wind speed range where the Ka band Doppler shift is reduced (see Figure 14b). However, this damping maximum is much more distinct than the maximum of the measured X band damping ratios. Again, our data show that the disappearance of bound Ka band Bragg waves gives rise to a damping maximum. Moreover, freely propagating Ka band Bragg waves on a slick-free water surface propagate with the same

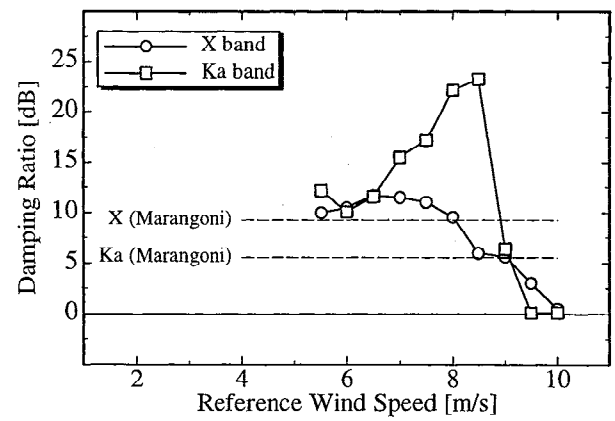

Figure 15. Wind speed dependence of the damping ratios, that is, the ratios of the backscattered radar power from a slick-free and a slick-covered water surface. The circles refer to X band data, and the squares refer to Ka band data. The dashed horizontal lines denote theoretical values for the damping of (freely propagating) Bragg waves following Marangoni damping theory [*Hühnerfuss,* 1986].

phase velocity (31.4 cm/s) as gravity waves with a frequency of 5.4 Hz. Since the latter are strongly damped by the OLA slick, we hypothesize that the observed damping maximum at Ka band is a manifestation of the existence of higher order harmonics of the (parent) 5.4 Hz gravity waves. If these gravity waves are damped by the OLA slick, we may expect that the Ka band Doppler shifts are reduced and that the damping ratios at Ka band are increased, both of which have been observed in our experiments.

The results obtained from the slick-covered water surfaces show that depending on the wind speed, the same surface-active substance dampens the bound and freely propagating Bragg waves differently; at moderate wind speeds (approximately 6 m/s) the gravity waves are steep enough to generate bound X and Ka band Bragg waves, whereas in the wind speed range between 7 and 9 m/s, they are strongly damped (and therefore also are the bound Bragg waves). One possible explanation for our observation, that the damping ability of a surface-active substance strongly varies with increasing wind speed, is the morphology effect [*Hühnerfuss et al.*, 1994, 1996]: Owing to a different distribution of the film molecules on the water surface and, as a result, to their different interaction, the viscoelastic properties of the same substance, and thus its damping behavior, can change. Obviously, the conditions in the wind-wave tank at wind speeds between 7 and 9 m/s are optimum for the damping of the short gravity waves by OLA; that is, only freely propagating Bragg waves are generated.

6. Summary and Conclusions

Measurements of the wave amplitude and slope and of the radar backscatter at X and Ka band have been carried out in a wind-wave tank with mechanically generated gravity waves as well as with wind-generated waves on a slick-free and a slick-covered water surface. They have shown that the excitation of bound (parasitic) gravity-capillary and capillary waves results in a strong change of the wave slope (and wave height) spectra, particularly, in the transition from a quasi-discrete to a continuous spectrum. The dependencies of the X and Ka band relative backscattered power on the amplitude of the mechanically generated waves with wavelengths less than 30 cm, corresponding to frequencies higher than approximately 2.5 Hz, show a strong increase when the amplitude of the mechanically generated waves reaches a threshold value, thus confirming that the backscattering can be associated with bound harmonics at X band and with bound capillary waves at Ka band. The occurrence of bound X and Ka band Bragg waves traveling at the phase velocity of the gravity waves was also shown by our measurements of the radar Doppler shifts. Steep gravity waves with wavelengths longer than approximately 30 cm, corresponding to frequencies lower than 2.5 Hz, cannot effectively generate bound capillary waves. The Ka band backscattering is then determined by the breaking of the steep gravity waves, and for X band it is caused by both bound harmonics and wave breaking.

The results of our measurements with mechanically generated waves agree with those performed with wind-generated waves: It can be concluded from the radar Doppler spectra that the X band backscattering from a slick-free water surface at low wind speeds (up to approximately 4.5 m/s) and long fetches (15.5 m in our investigation) is determined mainly by bound waves, whereas the Ka band backscatter is caused by both bound and freely propagating Bragg waves. For wind speeds higher than 4.5 m/s the X band backscattering in our experiments is caused by both parasitic harmonics and freely propagating Bragg waves, whereas the Ka band backscatter is caused mainly by freely propagating Bragg waves. In particular, the generation of freely propagating wind waves results in a reduction of the X band Doppler shift at wind speeds of 4.5-5 m/s, which is less distinct at Ka band.

When comparing the results obtained by different authors, one has to take into account the different experimental setups, which may lead to different results. In particular, the existence of bound (Bragg) waves does not only depend on the wind speed and frequency of the gravity waves but also, for example, on the fetch length and the wave age (which may strongly differ in different experimental setups). We suspect that even on the open ocean, X and Ka band Bragg waves are both freely propagating and bound to gravity waves (which in turn may be modulated by the long ocean waves).

The measurements of the X and Ka band backscatter from wind-generated waves on a water surface covered with oleyl alcohol (OLA) have shown that the coverage of the water surface with a surface-active substance has a strong influence on the generation of bound waves at the crests of the gravity waves. At intermediate wind speeds of approximately 6 m/s the X band backscatter is mainly caused by bound Bragg waves, and the Ka band backscatter is mainly caused by both bound and freely propagating Bragg waves. In the wind speed range between 7 and 9 m/s, where the short gravity waves are strongly damped by the OLA slick, both the X and Ka band backscatter are caused only by freely propagating waves. This wave damping behavior of the OLA slick can explain the maximum damping of the radar backscatter in this particular wind speed range as well as the fact that the measured wave damping exceeds the values predicted by Marangoni damping theory for this (water wave) frequency range.

The results in section 5.3 obtained from a slick-covered water surface can be of great importance for the interpretation of measured reductions of the radar backscattering by oceanic surface films [*Hühnerfuss et al.*, 1994, 1996; *Wismann et al.*, 1998; *Gade*, 1996; *Gade et al.*, 1998b]. However, results obtained from wind-wave tank experiments cannot be readily transferred to the open ocean. Moreover, the described effects are obviously strongly dependent on the measurement conditions (i.e., on the fetch and the tank dimensions), so that only field experiments (e.g., similar measurements of the radar backscattering performed on the open ocean) can prove our assumption that bound Bragg waves have an important impact on the measured radar signal from the ocean surface. At least, taking our results into account, we can expect reductions of the radar backscatter at X, Ku, and Ka band that are higher than those predicted by Marangoni damping theory (assuming Bragg scattering). This has indeed been observed in various field experiments [*Wismann et al.*, 1998; *Gade*, 1996; *Gade et al.*, 1998b]. Assuming that the small Bragg waves on the open ocean may also be both bound and freely propagating, we conclude that our results are also of importance for the interpretation of field experiments with oceanic surface films.

Acknowledgments. One of the authors (S.E.) would like to thank the Institute of Oceanography and the Institute of Organic Chemistry of the University of Hamburg for the arrangement of his visits to Hamburg and for the kind hospitality offered to him during these

visits. This work has been supported by the German Space Agency (DARA) under contract 01QS9016/50QS90165, by the German Science Foundation (DFG) under contract Hu583/1-2, and by the Fraunhofer Gesellschaft, München (contract T/RF35/L0013/ L1309 SAXON-FPN).

References

Alpers, W., and H. Hühnerfuss, The damping of ocean waves by surface films: a new look at an old problem, *J. Geophys. Res., 94,* 6251–6265, 1989.

Apel, J.R., An improved model of the ocean surface wave vector spectrum and its effects on radar backscatter, *J. Geophys. Res., 99,* 16,269–16,291, 1994.

Benjamin, T.B., and J.E. Feir, The disintegration of wave trains on deep water, 1, Theory, *J. Fluid Mech. 27,* 414–430, 1967.

Chang, J.H., R.N. Wagner, and H.C. Yuen, Measurement of high frequency capillary waves on steep gravity waves, *J. Fluid Mech., 86,* 401–413, 1978.

Cini, R., and P.P. Lombardini, Damping effect of monolayers on surface wave motion in a liquid, *J. Colloid Interface Sci., 65,* 387–389, 1978.

Cini, R., P.P. Lombardini, and H. Hühnerfuss, Remote sensing of marine slicks utilizing their influence on wave spectra, *Int. J. Remote Sens., 4,* 101–110, 1983.

Cox, C.S., Measurements of slopes of high-frequency wind waves, *J. Mar. Res., 16,* 199–225, 1958.

Crapper, G.D., Non-linear capillary waves generated by steep gravity waves, *J. Fluid Mech., 40,* 149–159, 1970.

Donelan, M.A., and W.H. Hui, Mechanics of ocean waves, in *Surface Waves and Fluxes,* vol.1, edited by G.L. Geernaert and W.J. Plant, pp. 209–246, Kluwer Acad., Norwell, Mass., 1990.

Duncan, J.R., W.C. Keller, and J.W. Wright, Fetch and wind speed dependence of Doppler spectra, *Radio Sci., 9,* 809–819, 1974.

Ebuchi, N., H. Kawamura, and Y. Toba, Fine structure of laboratory wind wave surfaces studied using an optical method, *Boundary Layer Meteorol., 39,* 133–151, 1987.

Ebuchi, N., H. Kawamura, and Y. Toba, Statistical properties of microwave backscattering from laboratory wind wave surfaces, *J. Oceanogr., 48,* 139–154, 1992.

Ebuchi, N., H. Kawamura, and Y. Toba, Physical processes of microwave backscattering from laboratory wind wave surfaces, *J. Geophys. Res., 98,* 14,669–14,681, 1993.

Ermakov, S.A., E.M. Zujkova, A.R. Panchenko, S.G. Salashin, T.G. Talipova, and V.I. Titov, Surface film effect on short wind waves, *Dyn. Atmos. Oceans, 10,* 31–50, 1986.

Ermakov, S.A., K.D. Ruvinsky, and S.G. Salashin, Local relation between ripples on gravity-capillary wave crests and their curvature, *Izv. Acad. Sci. USSR Atmos. Oceanic Phys., Engl. Transl., 24,* 561–563, 1988.

Feindt, F., Radar-Rückstreuexperimente am Wind-Wellen-Kanal bei sauberer und filmbedeckter Wasseroberfläche im X band (9.8 GHz), Ph.D. dissertation, Fachbereich 15 (Geowissenschaften), 224 p., Univ. of Hamburg, Hamburg, Germany, 1985.

Gade, M., Untersuchungen zur Abbildung biogener und anthropogener Oberflächenfilme auf dem Meer mit Hilfe von Radarsensoren, Ph.D. dissertation, Fachbereich 15 (Geowissenschaften), 176 p., Univ. of Hamburg, Hamburg, Germany, 1996.

Gade, M., W. Alpers, H. Hühnerfuss, and P.A. Lange, Wind-wave tank measurements of wave damping and radar cross sections in the presence of monomolecular surface films, *J. Geophys. Res., 103,* 3167–3178, 1998a.

Gade, M., W. Alpers, H. Hühnerfuss, H. Masuko, and T. Kobayashi, The imaging of biogenic and anthropogenic ocean surface films by the multifrequency/multipolarization SIR-C/X-SAR, *J. Geophys. Res.,* in press, 1998b.

Gade, M., W. Alpers, H. Hühnerfuss, V.R. Wismann, and P.A. Lange, On the reduction of the radar backscatter by oceanic surface films: scatterometer measurements and their theoretical interpretation, *Remote Sens. Environ.,* in press, 1998c.

Graf, K.A., D.E. Tremain, and H. Guthart, Induced-current effects on microwave backscatter, *IEEE Trans. Antennas Propag., AP-25,* 36–44, 1977.

Hühnerfuss, H., The molecular structure of the system water/monomolecular surface film and its influence on water wave damping, Habilitationsschrift, Fachbereich 13 (Chemie), 245 p., Univ. of Hamburg, Hamburg, Germany, 1986.

Hühnerfuss, H., P.A. Lange, J. Teichert, and H. Vollmers, A wind wave tunnel for the investigation of artificial slick wave damping and drift, *Meer. Mar. Tec., 7,* 23–26, 1976.

Hühnerfuss, H., W. Alpers, P.A. Lange, and W. Walter, Attenuation of wind waves by artificial surface films of different chemical structure, *Geophys. Res. Letters, 8,* 1148-1186, 1981.

Hühnerfuss, H., P.A. Lange, and W. Walter, Wave damping by monomolecular surface films and their chemical structure, 1, Variation of the hydrophobic part of carboxylic acid esters, *J. Mar. Res., 40,* 209–225, 1982.

Hühnerfuss, H., W. Alpers, O. Fäst, P.A. Lange, A. Loffet, K. Richter, R.C. Schriel, N. Skou, and F. Witte, The discrimination between crude oil spills and monomolecular sea slicks by airborne remote sensors, in The Archimedes 2 experiment, Joint Research Center Report, Ispra, Italy, 167–177, 1987.

Hühnerfuss, H., A. Gericke, W. Alpers, R. Theis, V. Wismann, and P.A. Lange, Classification of sea slicks by multi-frequency radar techniques: new chemical insights and their geophysical implications, *J. Geophys. Res., 99,* 9835–9845, 1994.

Hühnerfuss, H., W. Alpers, H. Dannhauer, M. Gade, P.A. Lange, V. Neumann, and V. Wismann, Natural and man-made sea slicks in the North Sea investigated by a helicopter-borne 5-frequency radar scatterometer, *Int. J. Remote Sens., 17,* 1567–1582, 1996.

Jähne, B., and K.S. Riemer, Two-dimensional wave number spectra of small-scale water surface waves, *J. Geophys. Res., 95,* 11,531–11,546, 1990.

Keller, W.C., T.R. Larson, and J.W. Wright, Mean speeds of wind waves at short fetch, *Radio Sci.,9,* 1091–1100, 1974.

Kwoh, D.S., and B.M. Lake, The nature of microwave backscattering from water waves, in *The Ocean Surface,* edited by Y. Toba and H. Mitsuyasu, pp. 249–256, D. Reidel, Norwell, Mass., 1985.

Lange, P.A., and H. Hühnerfuss, Horizontal surface tension gradients induced in monolayers by gravity water wave action, *J. Phys. Oceanogr., 14,* 1620–1628, 1984.

Lange, P.A., B. Jähne, J. Tschiersch, and I. Ilmberger, Comparison between an amplitude measuring wire and a slope-measuring laser water wave gauge, *Rev. Sci. Instrum., 53,* 651–655, 1982.

Lobemeier, P., Wire probe for measuring high frequency sea waves, *J. Fluid Mech., 16,* 138–159, 1981.

Longuet-Higgins, M.S., The generation of capillary waves by steep gravity waves, *J. Fluid Mech., 52,* 725–751, 1963.

Longuet-Higgins, M.S., Capillary rollers and bores, *J. Fluid Mech., 240,* 659–679, 1992.

Longuet-Higgins, M.S., and R.P. Cleaver, Crest instabilities of gravity waves, I, The almost-highest wave, *J. Fluid Mech., 258,* 115–129, 1994.

Longuet-Higgins, M.S., R.P. Cleaver, and M.J.H. Fox, Crest instabilities of gravity waves, II, Matching and asymptotic analysis, *J. Fluid Mech., 259,* 333–344, 1994.

Lucassen, J., Effect of surface-active material on the damping of gravity waves: A reappraisal, *J. Colloid Interface Sci., 85,* 52–58, 1982.

Mc Lean, J.W., Instability of finite-amplitude water waves, *J. Fluid Mech., 114,* 315–330, 1982.

Melville, W.K., A.D. Rozenberg, and D.C. Quigley, Laboratory study of polarized microwave scattering at grazing incidence, *Proc. Int. Geosci. Remote Sens. Symp., 15,* 951–953, 1995.

Mitsuyasu, H., and T. Honda, Wind-induced growth of water waves, *J. Fluid Mech., 123,* 425–442, 1982.

Perlin, M., H. Lin, and C.-L. Ting, On parasitic capillary waves generated by steep gravity waves: an experimental investigation with spatial and temporal measurements, *J. Fluid Mech., 255,* 597–620, 1993.

Phillips, O.M., *The Dynamics of the Upper Ocean,* Cambridge Univ. Press, New York, 1977.

Plant, W.J., A relationship between wind stress and wave slope, *J. Geophys. Res., 87,* 1961–1967, 1982.

Plant, W.J., A model for microwave Doppler sea return at high incidence angles: Bragg scattering from bound, tilted waves, *J. Geophys. Res., 102,* 21,131–21,146, 1997.

Rozenberg, A.D., D.C. Quigley, and W.K. Melville, Laboratory study of polarized microwave scattering by surface waves at grazing incidence: The influence of long waves, *IEEE Trans. Geosci. Remote Sens., 34,* 1331–1342, 1996.

Ruvinsky, K.D., and G.I. Freidman, The generation of capillary–gravity waves by steep gravity waves, *Izv. Acad. Sci. USSR Atmos. Oceanic Phys., Engl. Transl. 17,* 548–553, 1981.

Ruvinsky, K.D., F.I. Feldstein, and G.I. Freidman, Numerical simulation of the quasi–stationary stage of ripple excitation by steep gravity–capillary waves, *J. Fluid Mech., 230,* 339–353, 1991.

Tokuda, M., and Y. Toba, Statistical characteristics of individual waves in laboratory wind waves, II, Self–consistent similarity regime, *J. Oceanogr. Soc. Jpn., 38,* 8–14, 1982.

Valenzuela, G.R., Theories for the interaction of electromagnetic and oceanic waves: A review, *Boundary Layer Meteorol., 13,* 61–85, 1978.

Wei, Y., and J. Wu, In situ measurements of surface tension, wave damping, and wind properties modified by natural films, *J. Geophys. Res., 97,* 5307–5313, 1992.

Wright, J.W., A new model for sea clutter, *IEEE Trans. Antennas Propag., AP–16,* 217–223, 1968.

W. Alpers and M. Gade, Institut für Meereskunde, Universität Hamburg, Troplowitzstrasse 7, D-22529 Hamburg, Germany. (e-mail: alpers@ifm.uni-hamburg.de; gade@ifm.uni-hamburg.de)

S.A. Ermakov, Institute of Applied Physics, Russian Academy of Sciences, 46 Ul'janov Street, 603600 Nizhny Novgorod, Russia. (e-mail: stas@hydro.appl.sci-nnov.ru)

H. Hühnerfuss, Institut für Organische Chemie, Universität Hamburg, Martin-Luther-King-Platz 6, D-20146 Hamburg, Germany. (e-mail: huehnerf@chemie.uni-hamburg.de)

P.A. Lange, Bundesanstalt für Wasserbau, Aussenstelle Küste, Wedeler Landstrasse 157, D-22559 Hamburg, Germany. (e-mail: lange@hamburg.baw.de)

(Received March 5, 1997; revised March 2, 1998; accepted March 9, 1998.)